Hindawi
Indoor Air
Volume 2024, Article ID 6642205, 13 pages
https://doi.org/10.1155/2024/6642205

Research Article

Existence of a Nonzero Worst-Case ACH for Short-Term Exposure in Ventilated Indoor Spaces

K. A. Krishnaprasad,[1] **N. Zgheib**,[2,3] **K. Choudhary**,[4] **M. Y. Ha**,[4] **C. Y. Choi**,[5] **K. S. Bang**,[5] **S. Jang**,[5] **and S. Balachandar**[1]

[1]*Department of Mechanical and Aerospace Engineering, University of Florida, Gainesville, FL 32611, USA*
[2]*Department of Mechanical Engineering, The University of Texas Rio Grande Valley, Edinburg, TX 78573, USA*
[3]*The University of Texas Rio Grande Valley Center for Advanced Manufacturing Innovation and Cyber Systems (CAMICS), Edinburg, TX 78573, USA*
[4]*School of Mechanical Engineering, Pusan National University, Pusan, Republic of Korea*
[5]*Home Appliance & Air Solution Company, LG Electronics, Seoul, Republic of Korea*

Correspondence should be addressed to S. Balachandar; bala1s@ufl.edu

Received 5 June 2023; Revised 9 September 2023; Accepted 8 March 2024; Published 26 March 2024

Academic Editor: Riccardo Buccolieri

A well-ventilated room is essential to reduce the risk of airborne transmission. As such, the scientific community sets minimum limits on ventilation with the idea that increased ventilation reduces pathogen concentration and thus reduces the risk of transmission. In contrast, the upper limit on ventilation is usually determined by human comfort and the need to reduce energy consumption. While average pathogen concentration decreases with increased ventilation, local concentration depends on multiple factors and may not follow the same trend, especially within short exposure times over large separation distances. Here, we show through experiments and high-fidelity simulations the existence of a worst-case ventilation where local pathogen concentration increases near the receiving host. This occurs during the type of meetings that were recommended during the pandemic (and in some cases solely authorized) with reduced occupancy adhering to social distancing and short exposure times below 20 minutes. We maintain that for cases of high occupancy and long exposure time, increased ventilation remains necessary.

1. Introduction

The recent pandemic has increased the general awareness of risk of transmission by airborne viruses in indoor settings [1–7]. With well-documented evidence of the disease explosively spreading from one sick to many susceptible individuals [8, 9], airborne transmission and the role of indoor ventilation have become the subject of intense investigation [10–17]. For airborne transmission, the virus-laden droplets ejected by the sick individual through breathing, talking, coughing, or sneezing, rapidly evaporate and precipitate as virus-containing droplet nuclei. While larger droplets rapidly settle down, smaller nuclei remain airborne for hours and can spread to far corners, potentially infecting others.

ASHRAE standards 62-1 [18] provides guidelines for acceptable ventilation and indoor air quality. They prescribe a minimum ventilation flow rate per person in the range of 2.5-5 liters per second per person depending upon the occupancy density for nonresidential indoor spaces. These guidelines are intended to maintain basic indoor air quality and reduce the risk of airborne transmission below an acceptable level. While operating above a minimum threshold for ventilation rate is effective for the majority of situations in which occupancy levels are high and exposure times are long, our findings indicate that in certain situations of social distancing and short exposure time, the standard recommendations may have an adverse effect and may inadvertently enhance the risk of transmission.

The volumetric concentration of airborne nuclei within an indoor space is of paramount importance in determining the risk of transmission. The nucleus concentration depends primarily on the balance between the rate at which they are exhaled by the sick individual and the rate at which they are removed by ventilation and slow sedimentation. Based on this simple balance, it is commonly recommended that air conditioning units be operated at as high a fan setting, i.e., with as large a value of air changes per hour (ACH), as human comfort or cost of operation will permit [19–22]. The benefits of good ventilation, either in terms of natural cross-breeze with open windows or air conditioning at a high enough setting without recycling of contaminated air, are quite clear. Nevertheless, our recent investigation of turbulent dispersal of virus-laden nuclei has revealed a surprising result that when a susceptible individual shares an indoor space with a sick individual for a short duration, there exists a worst-case ventilation setting (i.e., a least favorable ACH), which maximizes the infectious quanta inhaled by the susceptible.

Although this prediction has been briefly observed in an experimental study by Ai et al. [23], the mechanisms behind this observation, which can be anticipated with some reflection, have not been reported in detail. At low values of ACH, due to slow mixing, the probability of the infectious nuclei being transported over longer distances across the room during a short-time span is low. At moderately high values of ACH, while the room-averaged pathogen concentration is reduced, the probability of spreading across the room in a short time increases, due to more rapid spreading. When ACH is increased beyond the worst-case value, though room-scale mixing is rapid, the steady-state pathogen concentration decreases, and therefore, the effect of increased ventilation follows the expected behavior of reduced inhalation of infectious quanta. The existence of the worst-case ACH is therefore related to a competition between rapid mixing and lower steady-state concentration. Thus, to avoid operating under the worst-case scenario for viral contagion, one must prevent efficient mixing across the room between the sick and susceptible through individualized microventilation. If that is not an option, it is better to turn off the air conditioner (AC) or fan during the short meeting to prevent airborne spreading. Such recommendations could be of relevance to specific scenarios where the sick and the susceptible are well-separated and remain together for a brief period of $\mathcal{O}(20)$ minutes or less. Such scenarios are encountered during a patient/doctor, client/lawyer, or borrower/banker meeting in a consulting room.

In this paper, we investigate the validity of this interesting observation and present simple improved recommendations for reducing the risk of transmission in such scenarios. Numerous studies [6, 24, 25] have emphasized the significance of higher values of ACH in the context of long-term indoor airborne viral transmission, where extended exposure plays a more crucial role compared to accelerated dispersal resulting from increased air velocities. We would like to emphasize that the objectives and conclusions of our study are strictly limited to scenarios involving short occupancy times. Our findings are based on examining 25 million combinations of possible locations between a sick and a susceptible person in a canonical room of square plan form of size $L \times L \times 0.32L$ [26, 27]. This has been achieved in the context of high-fidelity large eddy simulations (LES), using a novel statistical overloading technique which has been presented in Methods. Other room and ventilation configurations have also been studied using the aforementioned statistical framework, but in the context of simulations by the lower-fidelity Reynolds-averaged Navier-Stokes (RANS) framework. The importance of flow patterns and paths in alleviating the spread of airborne diseases, especially in nosocomial settings [28], has been well-established. The aim of this study, however, is to analyze the cases where the location of a sick or susceptible person cannot be predetermined. In this scenario, the mean behavior of droplet dispersal at a chosen separation distance is analyzed using our statistical overloading technique.

The findings of our study indicate that for small to medium-sized indoor spaces, i.e., for spaces of volume under approximately $150\,\mathrm{m}^3$, operating the AC at the worst-case ACH could pose a significantly higher risk of infection, when social distancing guidelines are followed. This recommendation also applies to larger rooms, with volumes greater than approximately $200\,\mathrm{m}^3$, but the increased risk of infection at the worst-case ACH decreases with room size. We hasten to clarify the importance of the current finding by clearly stating that for other circumstances, where the separating distance is not large and the time of exposure is long, higher ACH is always recommended and a worst-case ACH does not exist.

2. Methods

Well-mixed models [6, 29–31] based on the well-mixed assumption have been widely used to predict the spread of infectious diseases in indoor spaces. The well-mixed assumption is rooted in the important fact that the flow within indoor spaces is turbulent and the turbulence promotes mixing of the airborne nuclei resulting in a well-mixed indoor environment. We leverage the statistical framework posited by Salinas et al. [26] and Krishnaprasad et al. [27] as the basis for this paper. The results presented here use their turbulence-informed statistical framework, developed entirely using computational methods, to act as an improvement on the well-mixed models. The key idea behind the concept of statistical overloading is that the one-way coupled nature of droplet dispersal allows for overloading the computational domain with millions of droplets of various sizes. This enables the computation of statistically significant two-point concentration statistics for any pair of source-sink locations within the given domain. The framework utilizes large eddy simulations (LES) and Reynolds-averaged Navier-Stokes (RANS) simulations of flow in indoor ventilated spaces combined with Lagrangian tracking of suspended droplets to provide statistics.

2.1. LES. The gas-phase LES governing equations are the filtered incompressible Navier-Stokes equations. The filtering process of the momentum equation introduces a subgrid

Reynolds stress term, which has been closed with the eddy viscosity model, where the turbulent eddy viscosity is obtained using the dynamic Smagorinsky model. These equations are solved using a highly scalable spectral element solver. The domain is discretized using $60 \times 60 \times 16$ hexahedral elements with 6^3 Gauss-Lobatto-Legendre (GLL) grid points within each element, which results in a total of 12.4 million grid points. A Dirichlet boundary condition for velocity is imposed at the inlet planes, while an open boundary condition is used at the outlet [32]. No-slip and no-penetration conditions are used at the lateral walls, floor, and ceiling. The turbulent flow reaches a statistically steady state before introducing nuclei to the simulation. For more details, we refer the reader to Salinas et al. [26].

The droplet nuclei are one-way coupled so that the nuclei do not modify the surrounding airflow. Nucleus-nucleus collisions are neglected, and nuclei are assumed to have deposited on a surface upon impact, i.e., the collision of a droplet nucleus with a solid surface results in the nucleus depositing on the surface at the place of collision. The present simulations track droplet nuclei that remain airborne following an expiratory event. Each droplet nucleus is individually tracked with its Lagrangian governing equations. The droplet motion is calculated using the quasisteady and gravity-buoyancy forces. The fluid velocity evaluated at the droplet nucleus center requires an additional contribution from unresolved subgrid eddies. The perturbation velocity is computed using the Langevin model. For specific details on its implementation, please refer to Salinas et al. [26]. For nuclei smaller than $10\,\mu$m, inertial effects are negligible, and the equilibrium-Eulerian model is used, where the nucleus velocities are obtained as the superposition of the fluid velocity at the nucleus center and the nucleus settling velocity [26].

2.2. RANS Simulations. In the RANS simulations, the flow is assumed to be turbulent and incompressible and the unsteady governing RANS conservation equations are solved to steady state [33] using the commercial code Ansys Fluent 19.2. The first-order implicit scheme is used for time integration with a second-order upwind scheme for the advection terms and the second-order centered scheme for the diffusion terms. A structured grid is generated throughout the computational domain, and a grid dependency test is performed to ensure that results are grid independent [33]. In addition, a turbulence model dependency test is also carried out by considering four different turbulent models, namely, k-ω, k-ε-realizable, k-ε-RNG, and k-ε-standard, and based on the results, further simulations were performed with k-ε-realizable model [33]. We implemented an enhanced wall treatment of turbulence for the near-wall region and used the pressure-based solver PRESTO for solving the pressure equation.

Droplet nucleus trajectories are computed using the discrete phase method (DPM) available in FLUENT. In the Lagrangian framework, the path of each airborne nucleus is evaluated by solving the equations of motion accounting for the drag and gravitational forces. The nucleus volume fraction is assumed to be negligible so that nuclei neither affect the flow within the room, nor the trajectory of other nuclei through possible collisions. The sub-micron-sized particles are modeled as tracer particles that follow the fluid flow with additional settling velocity. The RANS approach solves for only the ensemble-averaged velocity and does not solve for the total fluid velocity including the turbulent perturbations. Here, we use the continuous random walk model based on the normalized Langevin equation to estimate the turbulent velocity fluctuation along the particle trajectories.

2.3. Well-Mixed Model. The analysis in the statistical model [26, 27] is based on the well-mixed model developed by Bazant and Bush [6]. According to the well-mixed model, the entry of an infected person into a room increases the room-averaged nucleus concentration steadily and eventually, and a steady state is reached where the rate of emission by the infected person is balanced by the rate at which the nuclei exit the room.

According to the well-mixed model, for an infected person (source) with an exhalation rate of Q_b located within the room of volume $\mathscr{V}$, and considering $n_{so}(r)$ to be the concentration of exhaled virus-laden droplet nuclei of radius r that remain airborne, the time evolution of the well-mixed concentration $n_{\mathrm{wm}}(t, r)$ of droplet nuclei of radius r is given by

$$\mathscr{V}\frac{dn_{\mathrm{wm}}}{dt} = Q_b\, n_{so}(r) - \mathscr{V}\,\lambda_{\mathrm{wm}}\, n_{\mathrm{wm}}, \tag{1}$$

where the first term on the right-hand side accounts for the influx of droplet nuclei of radius r from the infectious source and the second-term accounts for the removal of droplet nuclei by the combined mechanisms of withdrawal through the outlet, settling down on the floors, and natural deactivation. The rate of removal is given by

$$\lambda_{\mathrm{wm}}(r) = \frac{\mathrm{ACH}}{3600} + \frac{V_s(r)}{H} + \lambda_{da}, \tag{2}$$

where $V_s(r)$, H, and λ_{da} represent the size-dependent droplet settling velocity, room height, and the exponential rate of viral deactivation, respectively. The viral deactivation rate, λ_{da}, is set at $0.3\,\mathrm{h}^{-1}$ [31, 34]. Here, ACH is the effective air changes per hour in the room.In the scenario where the infected person enters the room at $t = 0$, the droplet nucleus concentration within the room is initially zero and then experiences a gradual rise following the arrival, ultimately reaching a state of equilibrium concentration. We define the normalized well-mixed nucleus concentration within the room as $\hat{n}_{\mathrm{wm}}(t, r) = n_{\mathrm{wm}}(t, r)/(Q_b n_{so}(r))$. As a result of the normalization, $\hat{n}_{\mathrm{wm}}$ can be interpreted as the number of nuclei of size r per unit volume of air for a unit ejection rate by the source. Thus, the normalization has the advantage that it removes the dependence on the details of the expiration activity of the source. The time evolution of normalized well-mixed nucleus concentration is expressed as [6, 26, 29–31]

$$\hat{n}_{\mathrm{wm}}(t, r) = \frac{1}{\lambda_{\mathrm{wm}}(r)\,\mathscr{V}}\left(1 - e^{-\lambda_{\mathrm{wm}}(r)\,t}\right). \tag{3}$$

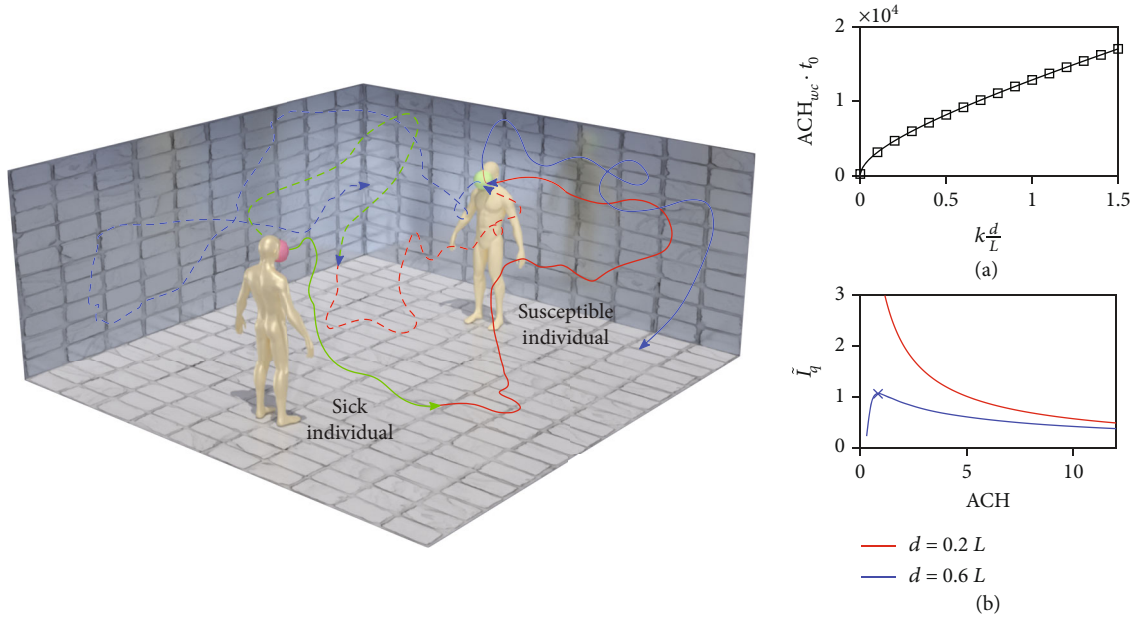

FIGURE 1: Schematic of two sample trajectories (solid and dashed lines) of airborne nuclei traveling from one possible combination of a sick to a susceptible individual. For short-time exposure, the green-colored portion corresponds to the trajectory followed at a low value of ACH. The continued red-colored portions correspond to trajectories for worst-case ACH. The continued blue-colored portions correspond to even higher ACH. (a) Theoretical prediction of the product $\mathrm{ACH}_{\mathrm{wc}}\, t_0$ plotted as a function of scaled distance $k\, d/L$. (b) Normalized quanta inhaled (obtained from LES) plotted against ACH for two sick-susceptible combinations of $d = 0.6L$ and $d = 0.2L$. In the former scenario, there is a clear worst-case ACH, whereas no such worst-case ACH exists for the latter.

The size-weighted average of the normalized nucleus concentration is given by

$$\overline{\widehat{n}_{\mathrm{wm}}}\,(\tau) = \frac{\int_0^{r_c} \widehat{n}_{\mathrm{wm}}(\tau, r)\, V(r)\, Q_b\, n_{so}(r)\, dr}{\int_0^{r_c} V(r)\, Q_b\, n_{so}(r)\, dr}, \tag{4}$$

where $V(r)$ is the volume of a droplet nucleus of radius r and the upper limit of the integral, r_c, is the critical droplet radius [6]. The ejected spectra $n_{so}(r)$ are taken from the experimental measurements of Morawska et al. [35].Following Buonanno et al. [36], the rate of inhalation of quanta, $\mathrm{IR}_{q,\mathrm{wm}}$ (for the well-mixed model), can be written as a function of $\overline{\widehat{n}_{\mathrm{wm}}}$ in the form

$$\mathrm{IR}_{q,\mathrm{wm}} = \underbrace{\mathrm{ER}_q}_{\text{source}}\ \underbrace{\overline{\widehat{n}_{\mathrm{wm}}}\,(\tau)}_{\text{wm–tf}}\ \underbrace{\mathrm{IR}}_{\text{sink}}, \tag{5}$$

where ER_q is the rate of exhalation of infectious quanta (measured in quanta per second) by the source and IR is the inhalation rate of the exposed subject (measured in cubic meter per second). Thus, $\overline{\widehat{n}_{\mathrm{wm}}}$ can be inferred as the *well-mixed transfer function* (wm-tf) that accounts for the fraction of what got ejected at the source that becomes available at the sink. Assuming that the number of infectors is 1, ER_q can be calculated as $\mathrm{ER}_q = c_v\, c_i\, \mathscr{V}_{\mathscr{R}}$, where c_v is the viral load in the sputum measured as RNA copies per milliliter, c_i is the conversion factor that converts the viral load to infectious quantum, and $\mathscr{V}_{\mathscr{R}} \sim \int_0^{r_c} V(r)\, Q_b\, n_{so}(r)\, dr$ is the total volume of airborne droplet nuclei ejected in milliliter per second.

2.4. Improvement to the Well-Mixed Model. As shown in [26, 27], the theory can provide really accurate predictions of the nucleus concentration at the room scale. However, the accuracy of the theory falls considerably when we consider the separation distance between the source and the sink. For example, nucleus concentrations, according to the statistical framework, for source-sink separations under 2 m are predicted to be, on average, nearly two times higher than the concentration predicted by the well-mixed theory.

To overcome this shortcoming, Salinas et al. [26] proposed a separation distance-specific normalized nucleus concentration, $\langle \widehat{n} \rangle_d(\tau, r)$, defined as the nucleus concentration averaged over all source and sink combinations separated by a separation distance, d. This entailed evaluating droplet nucleus concentrations for 25 million combinations of source and sink locations within their domain. The quantity, $\langle \widehat{n} \rangle_d(\tau, r)$, is then obtained by averaging the concentrations across all source and sink locations that were separated by the specified distance, d. Similar to Eq. (4), the size-weighted average of the separation distance-specific normalized nucleus concentration is given by

$$\overline{\langle \widehat{n} \rangle_d}\,(\tau) = \frac{\int_0^{r_c} \langle \widehat{n} \rangle_d(\tau, r)\, V(r)\, Q_b\, n_{so}(r)\, dr}{\int_0^{r_c} V(r)\, Q_b\, n_{so}(r)\, dr}. \tag{6}$$

To preserve the simplicity of the well-mixed theory while incorporating the addition of separation distance into the

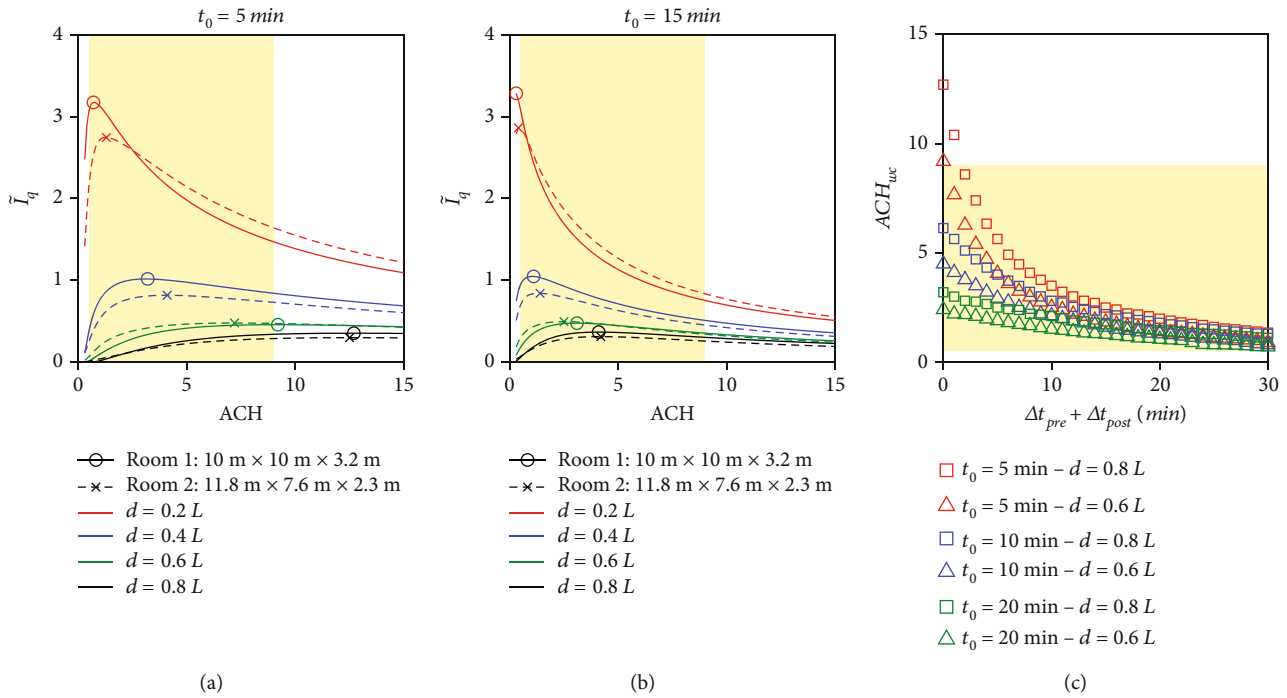

FIGURE 2: (a, b) Normalized quanta obtained from LES as a function of ACH for separations of $0.2L$, $0.4L$, $0.6L$, and $0.8L$ for overlap times of $t_0 = 5$ and 15 min, respectively. The peaks (marked by a circle for room 1 and a cross for room 2) clearly highlight the worst value of ACH to be avoided. (c) Plots of ACH_{wc} as a function of $\Delta t_{pre} + \Delta t_{post}$ for three different values of t_0 and for two different values of large sick-to-susceptible separation. All cases contain a yellow band to depict the realistic range of ACH values for a typical classroom or office space.

fold of the existing theory, a simple multiplicative transient correction function $\gamma(\tau, d)$ is provided.

$$\gamma(\tau, d) = \frac{\overline{\langle \hat{n} \rangle_d}(\tau)}{\overline{\hat{n}_{\text{wm}}}(\tau)}. \tag{7}$$

The advantage of this definition of the correction function is that it greatly simplifies the complex manner in which the room-scale flow causes the infectivity to deviate from the well-mixed theory into a single function that can be used in conjunction with the well-mixed model while improving upon it. The rate of inhalation of quanta that accounts for the source-sink separation distance, IR_q, can then be written as

$$\text{IR}_q = \underbrace{\text{ER}_q}_{\text{source}} \underbrace{\overline{\hat{n}_{\text{wm}}}(\tau)\gamma(\tau, d)}_{\text{2-pt tf}} \underbrace{\text{IR}}_{\text{sink}}, \tag{8}$$

where the *two-point transfer function* (2-pt tf) accounts for the separation between the source and the sink. While the simulations performed by Salinas et al. [26] considered three different values of ACH, the statistically converged results yielded a clear power-law scaling allowing us to predict the results for a wider range of ACH values.

2.5. Cumulative Exposure at the Sink. The total quanta inhaled over a period of time or the dose will be the time integral of IR_q, and it provides a good measure of the probability of an infection. This quantity, assuming the ejection rate of the source and the inhalation of the sink to be constant over time, can be defined as

$$I_q(t) = \text{ER}_q\, \overline{\mathscr{D}_d}(t)\, \text{IR}, \tag{9}$$

where $\overline{\mathscr{D}_d}(t)$ represents the cumulative exposure at the sink for the separation distance d between the source and the sink. As will be defined below, this quantity is obtained from a time integral of $\overline{\langle \hat{n} \rangle_d}(\tau)$. It is worth noting that the risk of infection can be evaluated within the Wells-Riley framework as $P_I = 1 - \exp(-I_q)$.The normalized cumulative quantum is defined as

$$\tilde{I}_q(t) = \frac{I_q(t)}{I_{q,\text{wm,ACH=1}}(t)}, \tag{10}$$

where $I_{q,\text{wm,ACH=1}}(t)$ is the total inhaled quanta predicted by the well-mixed theory for ACH = 1, which can be evaluated as

$$I_{q,\text{wm,ACH=1}}(t) = \frac{\text{ER}_q \times \text{IR}}{\lambda_{\text{wm}}\mathscr{V}} \left(t - \frac{1 - e^{-\lambda_{\text{wm}} t}}{\lambda_{\text{wm}}}\right). \tag{11}$$

As a result of this normalization, $\tilde{I}_q(t)$ is independent of the virological and physiological details contained in ER_q and IR.

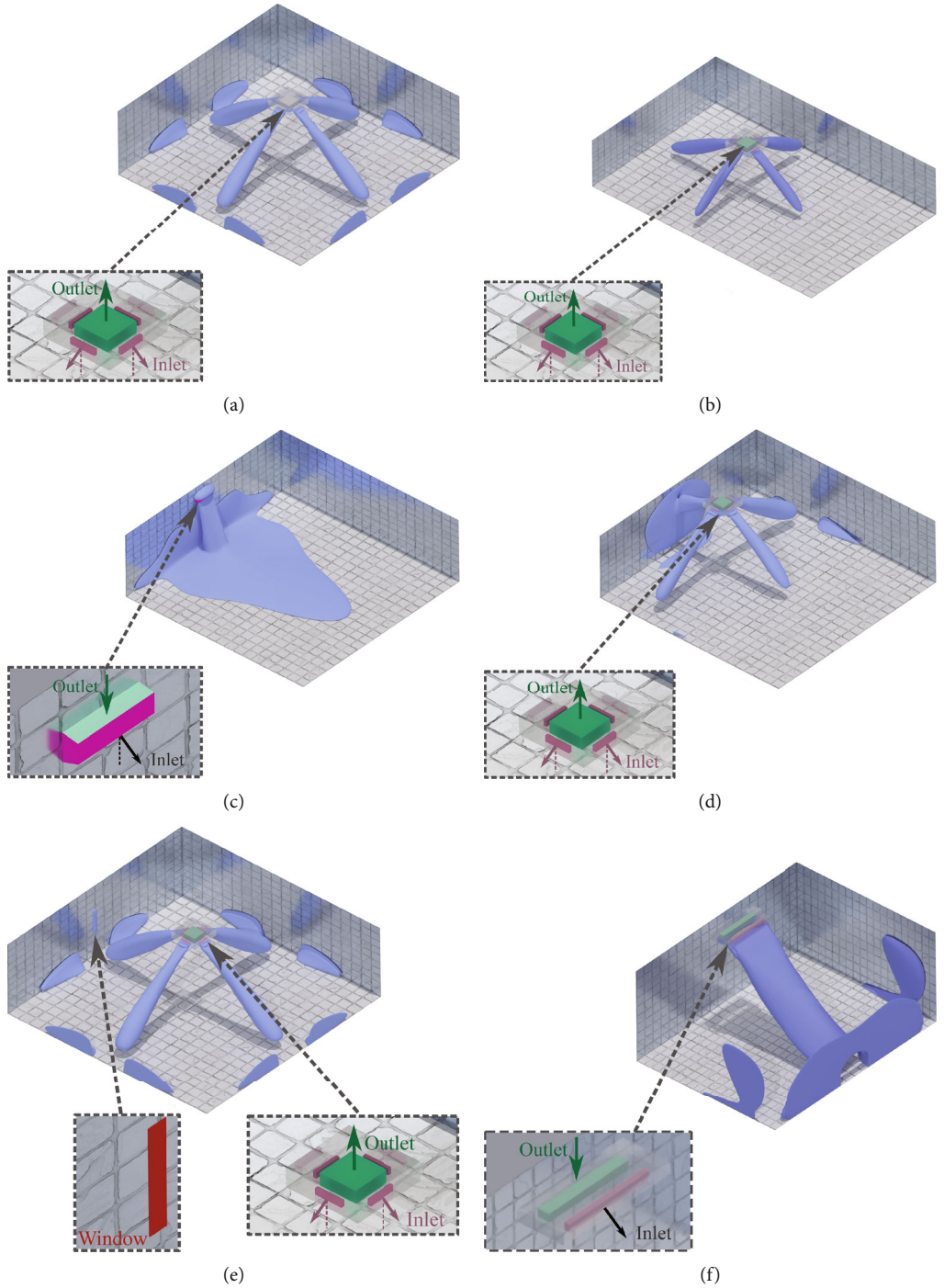

Figure 3: Layouts of the different geometries for which the simulations were performed along with the velocity magnitude isocontours of 0.6 m/s at ACH of 5 for rooms 1-5 and 0.5 m/s at ACH of 10 for room 6. (a) Room 1: 10 m × 10 m × 3.2 m room with a centrally located 4-way cassette air conditioning unit. (b) Room 2: 11.8 m × 7.6 m × 2.3 m room with a 4-way cassette air conditioning unit that is shifted 1.9 m from the center of the ceiling along the longer horizontal dimension and is central along the shorter horizontal dimension. (c) Room 3: 10 m × 10 m × 3.2 m room with a wall-mounted 1-way cassette air conditioning unit. (d) Room 4: 10 m × 10 m × 3.2 m room with a 4-way cassette air conditioning unit that is shifted 2.5 m from the center of the ceiling along one dimension. (e) Room 5: 10 m × 10 m × 3.2 m room with a centrally located 4-way cassette air conditioning unit and an open window. (f) Room 6: 4.5 m × 6 m × 2.7 m room with a wall-mounted 1-way cassette air conditioning unit.

Consider a simple scenario involving a specific count of occupants within an enclosed area possessing distinct geometry and predetermined attributes of the ventilation system. When examining the interplay between any single pairing of a source and a sink, we can simplify this problem into a function of five parameters—ACH, d, Δt_{pre}, t_0, and Δt_{post}.

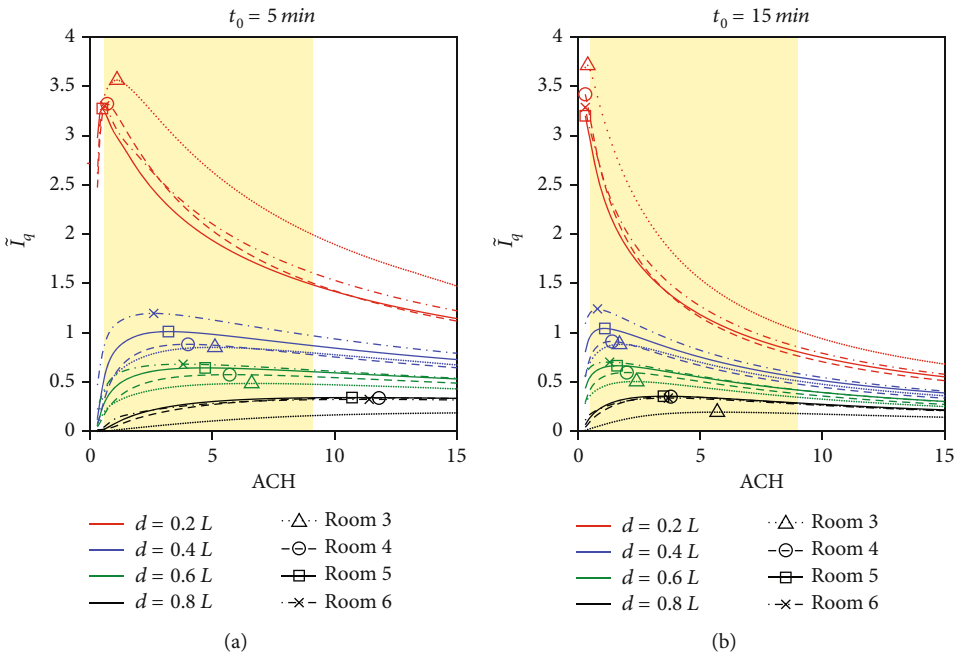

FIGURE 4: Normalized quanta obtained for different room and AC arrangements as a function of ACH for separations of $0.2L$, $0.4L$, $0.6L$, and $0.8L$ for overlap times of (a) $t_0 = 5$ and (b) 15 min. All cases display a peak highlighting the worst value of ACH to be avoided and a yellow band to depict a realistic range of ACH values for a classroom or an office space.

The parameters Δt_{pre}, t_0, and Δt_{post} are defined as the time of occupation of the source alone before the arrival of the sink, the time the source and sink spend together, and the time of occupation by the sink alone in the room after the departure of the source, respectively.

For the aforementioned scenario, the cumulative exposure at the sink can be expressed in terms of size-weighted normalized nucleus concentration as

$$\overline{\mathscr{D}_d}(t) = \int_0^t \overline{\langle \widehat{n} \rangle_d}(\tau)\, d\tau - \int_0^{\Delta t_{\text{pre}}} \overline{\langle \widehat{n} \rangle_d}(\tau)\, d\tau - \int_0^{\Delta t_{\text{post}}} \overline{\langle \widehat{n} \rangle_d}(\tau)\, d\tau, \tag{12}$$

where the total exposure time is defined as $t = \Delta t_{\text{pre}} + t_0 + \Delta t_{\text{post}}$. Using the relation (7), $\overline{\langle \widehat{n} \rangle_d}(\tau)$ can be evaluated in terms of the correction function $\gamma(\tau, d)$ and the well-mixed prediction $\overline{\widehat{n}_{\text{wm}}}(\tau)$ for any value of ACH and d from the statistical framework [26].

3. Results and Discussion

Figure 1 shows a schematic of two sample trajectories (a solid and a dashed line) of airborne nuclei traveling from one possible combination of a sick to a susceptible person within an indoor space. At small values of ACH and short exposure times, the path of the nuclei, shown in green, does not extend to the susceptible. As ACH is increased to its worst-case value, the exposure time is sufficient for the nucleus trajectories, continued in red, to extend up to the susceptible. With further increase in ACH, the nucleus trajectories, continued in blue, extend farther. Thus, below the worst-case ACH, the nucleus concentration at the susceptible is yet to fully build up during the short exposure time. Above the worst-case ACH, the exposure time is long enough for concentration build-up, but the built-up concentration decreases with increasing ACH.

The worst-case ACH can also be explained analytically by considering the scenario of the sick and the susceptible entering the room together and staying for an overlap time of t_0 seconds. Let the separation between the sick and the susceptible be d (in cases where there is a plastic barrier between the two, d is the shortest air path between the sick and the susceptible). The normalized quanta $\tilde{I}_q$ inhaled by the susceptible can be modeled as [6, 26, 29, 30, 35]

$$\tilde{I}_q = \frac{(\gamma_\infty/\text{ACH}) \int_{t_d}^{t_0} [1 - \exp\left(-(\text{ACH}/3600)\,[t - t_d]\right)] dt}{t_0 + [\exp\left(-t_0/3600\right) - 1]}. \tag{13}$$

The normalization factor in the denominator is the inhaled quanta as predicted by the well-mixed model for a unit ACH. The above model extends the well-mixed approximation [6, 29, 30, 35] in two important ways to account for the distance between the sick and the susceptible: (i) the correction function γ_∞ accounts for deviation from well-mixedness in the limit as $t_0 \longrightarrow \infty$. It has been observed that γ_∞ primarily depends on the normalized distance d/L and is largely independent of other factors such as ACH and the nature of ejection activity [26]. For distances $(d/L) > 0.45$, $\gamma_\infty < 1$ [26], indicating that for larger separations, long-time nucleus concentration is lower than the well-mixed prediction. Correspondingly, for shorter distances of $(d/L) < 0.45$, $\gamma_\infty > 1$. (ii) The quotient $[1 - \exp(-\text{ACH}$

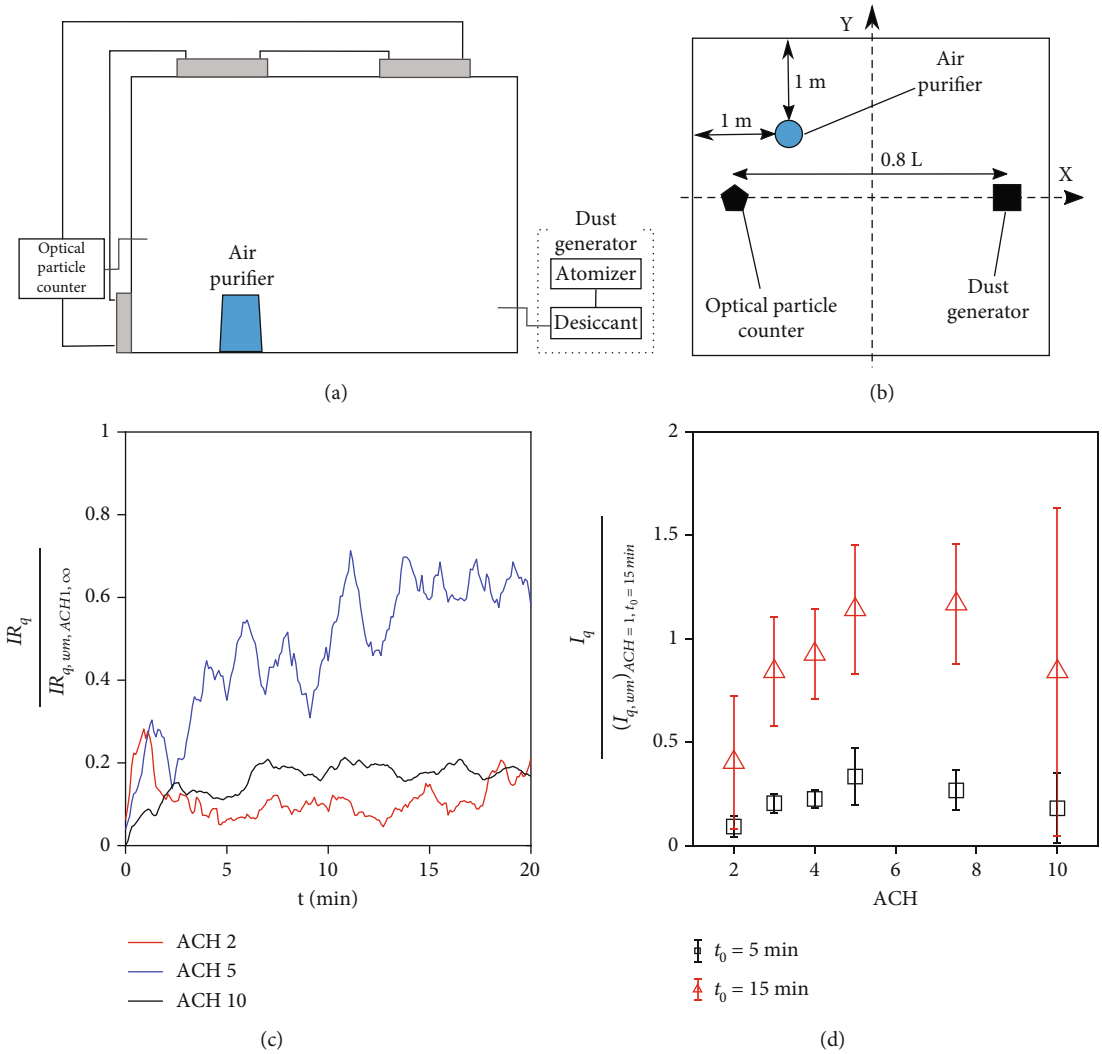

FIGURE 5: Experimental confirmation of the theoretical finding. (a) Schematic of the experimental setup. (b) Plan view of the experimental setup. (c) Time history of normalized quanta measured at the sensor for three different ACH values. (d) Time-integrated cumulative normalized quanta at the sensor as a function ACH. Integrated value for both 5 and 15 min shows a distinct peak identifying the worst-case ACH. The error bars indicate a one-sigma variation obtained from several repetitions of the experiments.

$(t - t_d)/3600)]$ accounts for the sigmoid-like increase in nucleus concentration at the susceptible location towards the long-time value, and the integral accounts for the total inhalation over the exposure time.

The key aspect of the above model is the average delay time t_d it takes for the ejected nuclei to travel the distance d. The average delay time can be estimated as $t_d = k\,d/(L\,(\mathrm{ACH}/3600))$, where the denominator is the average air velocity and k is an $\mathcal{O}(1)$ constant. Thus, when the sick and the susceptible are well separated within the room, it takes a while for the pathogen to start arriving, resulting in a delayed build-up of pathogen concentration.

It can be shown that the integral admits a maximum and the worst-case ACH scales as $\mathrm{ACH}_{wc} \propto 1/t_0$. Furthermore, the product $\mathrm{ACH}_{wc}\,t_0$ depends only on the scaled distance kd/L, which is plotted in Figure 1(a). For example, for a scaled distance of $kd/L = 0.4$, we obtain $\mathrm{ACH}_{wc} = 7130/t_0$, which for a 15-minute meeting between the sick and the susceptible yields a worst-case ACH of about 6. The worst-case is further illustrated in Figure 1(b) where the normalized quantum inhaled is plotted against ACH for the sick-susceptible combination separated by a distance $d = 0.8L$. Also shown is the corresponding result for another sick-susceptible combination of $d = 0.2L$. At closer separation, there is no worst-case scenario, and the inhaled quanta continue to decrease with ACH. As mentioned previously, this study is aimed at predicting the mean behavior in settings such as classrooms or office spaces, where the location of the source may not be predetermined. To indicate the realistic operating conditions of an AC in those settings, the range of typically observed values of ACH, observed in literature [37–39], has been denoted by a shaded band in subsequent figures.

The lines in Figures 2(a) and 2(b) correspond to the normalized quanta $\tilde{I}_q$ obtained from LES as a function of ACH for separations of $0.2L$, $0.4L$, $0.6L$, and $0.8L$ for overlap times of $t_0 = 5$ and 15 min, respectively. The solid and

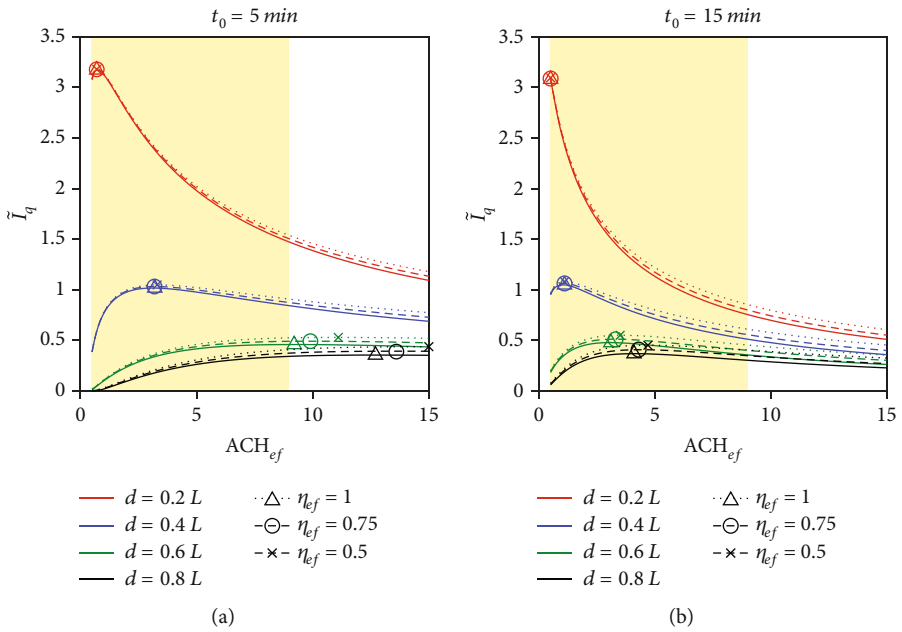

Figure 6: Normalized quanta obtained for room 1 as a function of ACH_{ef} for separations of $0.2L$, $0.4L$, $0.6L$, and $0.8L$ for overlap times of (a) $t_0 = 5$ and (b) 15 min. The curves are plotted for three filter efficiencies, $\eta_{ef} = 0.5$, 0.75, and 1. All cases display a peak highlighting the worst value of ACH_{ef} to be avoided. The yellow band depicts a realistic range of ACH values for a classroom or an office space.

dashed lines correspond to two different room geometries whose dimensions are indicated in the figure captions. The peaks in pathogen concentration (marked with a cross or an open circle) clearly highlight the worst value of ACH to be avoided. For overlap times in excess of 30 min and irrespective of the sick-to-susceptible separation distance, the ACH_{wc} is sufficiently small that increasing ACH is always beneficial. The computed actual behavior is in good agreement with the theoretical model presented above.

Figures 2(a) and 2(b) have been obtained assuming both the sick and the susceptible enter and leave the room simultaneously. However, we can envision scenarios where the sick has already been in the room for Δt_{pre} before the arrival of the susceptible, and the susceptible remains in the room for Δt_{post} after the departure of the sick. Note that the other two scenarios in which the susceptible arrives before the sick or the sick remains in the room after the susceptible has exited the room do not play a role in ACH selection.

Nonzero values of both pre- and postexposure times have qualitatively the same effect as increasing t_0. With increasing $\Delta t_{pre} + \Delta t_{post}$, although the inhaled quantum increases, the value of ACH_{wc} decreases. Therefore, for large enough $\Delta t_{pre} + \Delta t_{post}$, higher ACH values become favorable. Plots of worst-case ACH for the room 1 geometry as a function of $\Delta t_{pre} + \Delta t_{post}$ for three different values of t_0 are presented in Figure 2(c) for two different values of large sick-to-susceptible separation.

For any small consulting or conference room with a specified spatial separation between the two individuals, given good estimates of the overlap time t_0 and total exposure time $\Delta t_{pre} + t_0 + \Delta t_{post}$, Figure 2(c) can be consulted to identify the worst-case ACH to be avoided.

The above findings are not unique to the room being considered or to the specific placement of the air conditioning unit within the room. For example, Figures 2(a) and 2(b) also include the normalized quanta obtained for a rectangular room of different aspect ratio, and the results exhibit the same trend of worst-case ACH.

We have considered several other room configurations: (i) room 3: the same square room with a 1-way cassette AC mounted on one of the side walls; (ii) room 4: the same room as before but with the location of the 4-way cassette AC shifted to one side of the room; (iii) room 5: the same room as the one considered, but with an open window; and (iv) room 6: 4.5 m × 6 m × 2.7 m room with a wall-mounted 1-way cassette air conditioning unit [33]. The layouts for the various rooms are shown in Figure 3. The results for $t_0 = 5$ and 15 minutes, shown in Figure 4, are qualitatively similar and clearly exhibit a worst-case ACH when quantum inhaled by the susceptible is maximized. This indicates the robustness of the finding and insensitivity to details such as room shape, air conditioner type, and location. It is important to note that this finding is restricted to typical rooms where the horizontal aspect ratio of the room is $\mathcal{O}(1)$. For indoor settings like buses or trains, where the aspect ratio is much larger than 1, the validity of the model is yet to be tested.

As the final step, we validate the above theoretical and computational findings with laboratory experiments conducted at the indoor testing chamber of LG Electronics. A dust generator emitting potassium chloride droplets of radii ranging from 0.265 μm to 34 μm with a mean droplet radius

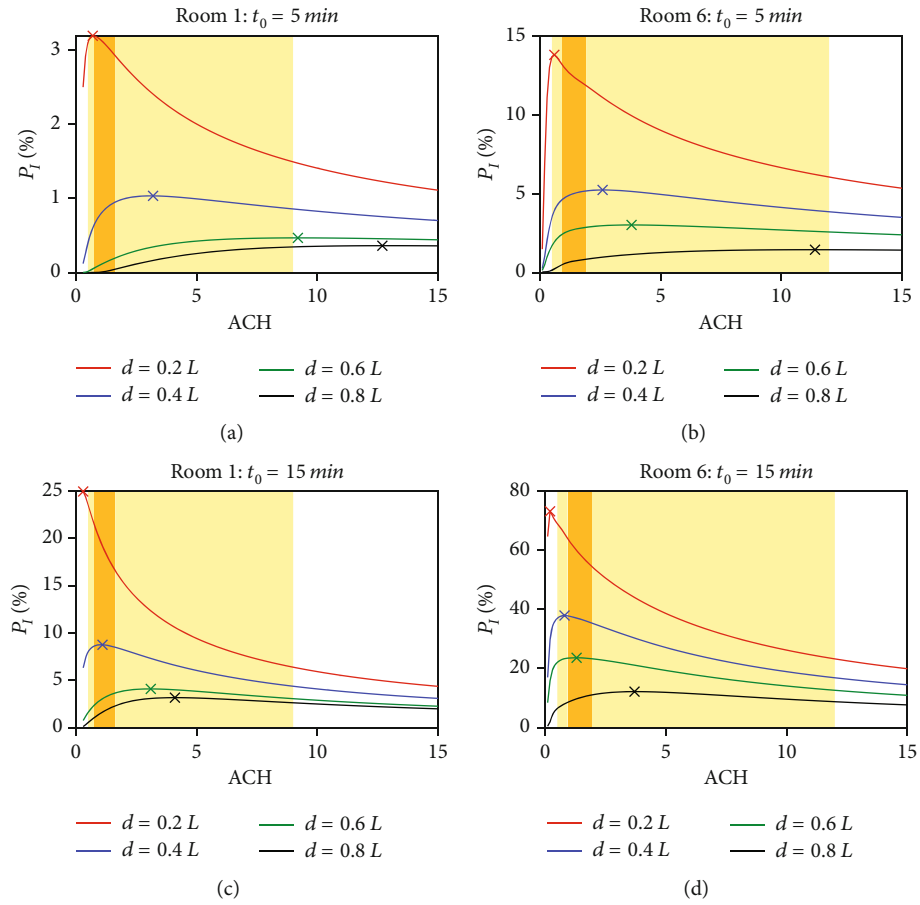

FIGURE 7: Risk of infection P_I obtained as a function of ACH for separations of $0.2L$, $0.4L$, $0.6L$, and $0.8L$ for overlap times of $t_0 = 5$ min for (a) room 1 and (b) room 6 and $t_0 = 15$ min for (c) room 1 and (d) room 6 ($ER_q = 970$ quanta/h; IR = 1 m^3/h [31]). All cases display a peak highlighting the worst value of ACH. The yellow bands depict a realistic range of ACH values in rooms 1 and 6. The orange bands depict the range of minimum ventilation rates prescribed by ANSI/ASHRAE Standard 62.1 (2022) for an occupancy of (a, c) 30 in room 1 and (b, d) 8 in room 6.

of 0.3 μm at a constant rate (10^9 droplets per minute) was placed in the chamber of size 3.65 m × 3.25 m × 2.35 m. The temperature and humidity inside the chamber were adjusted to 23°C and 55%, respectively. The inner wall of the chamber was made of an antistatic material to minimize the electrostatic attachment of particles. An optical particle counter (GRIMM's portable aerosol spectrometer model 1.109) was placed at a distance of $0.8L$ from the dust generator, where the length scale $L = (3.65 \times 3.25)^{1/2}$ m, to detect the concentration of airborne particles (see Figures 5(a) and 5(b)). The duster was set to run for 20 minutes while the sensor collected the concentration data. During this period, the air within the room was cleaned with an air purifier, and six different operating conditions of the purifier were considered with ACH values of 2, 3, 4, 5, 7.5, and 10. The values of ACH were obtained using the volume flow rates of air generated by the purifier, measured using 8 velocity sensors located at the outlet. These measures were found to be consistent with prior wind tunnel tests performed on the product. Figure 5(c) shows the total particle volume measured by the sensor integrated across the different sizes as a function of time. The level of fluctuation observed in Figure 5(c) is substantial due to the small size of the sensor volume, flow turbulence, and the chaotic nature of particle ejection. In the case of ACH = 2, the particle concentration is low but continues to steadily increase. At ACH = 10, a stationary state is quickly reached. At the intermediate ACH = 5, a stationary state is approached with a higher saturation concentration. These results are fully consistent with the theoretical model presented in equation (13). Figure 5(d) shows the cumulative concentration at the sensor location as a function of ACH for $t_0 = 5$ and 15 minutes, where the one-sigma error bar has been drawn from multiple repetitions of the experiments. A worst-case ACH can be clearly identified at both exposure times in Figure 5.

The results presented so far assume an air conditioning system with a perfect filter, i.e., an air conditioning system where all the pathogens passing through the outlet are removed and do not reenter the room through the inlet. However, this scenario is not realistic as most air conditioning systems recycle the air and do not perfectly filter the recycled air. In order to analyze the effect of filtration and recycling, we use the statistical framework that takes into consideration the effect of filtration [27]. The filtration efficiency of the air conditioning unit, η_{ef}, is defined as the fraction of particles that do not get recycled

back into the room through the ventilation unit. For a filter with $\eta_{ef} < 1$, the effective ACH of the ventilation unit can be defined as

$$\eta_{ef} = \frac{\mathrm{ACH}_{ef}}{\mathrm{ACH}}. \quad (14)$$

Figure 6 plots the normalized quanta inhaled against effective ACH for room 1 taking into account the effect of filter efficiency. We notice that, at larger relative separation distances ($d \geq 0.6L$) and low overlap times ($t_0 = 5$ min), there is a noticeable decrease in $\mathrm{ACH}_{wc,ef}$, with an increase in η_{ef}. As the overlap time increases and/or the separation distance decreases, the change in $\mathrm{ACH}_{wc,ef}$ with change in η_{ef} becomes negligible.

It is however important to note that, although the value of $\mathrm{ACH}_{wc,ef}$ stays relatively constant, the operating condition of an air conditioner is defined by the ACH, not ACH_{ef}. For instance, although the value of $\mathrm{ACH}_{wc,ef} \approx 3$ for the $\eta_{ef} = 0.5$, 0.75, and 1 for $d = 0.8L$ and $t_0 = 15$ minutes, this would correspond to ACH_{wc} values of approximately 6, 4, and 3, respectively, for the different filter efficiencies. Therefore, it is imperative that, in order to decide the optimal operating flow conditions of the ventilation system, or in this case, avoid the worst possible operating flow condition, a solid understanding of the efficiency of the filter being used is also desired.

The study so far demonstrates conclusively that a worst-case ACH exists for a typical ventilated indoor space, provided that the time of exposure is short and the separation distance relative to the size of the room is large. To quantify the risk of infection, the probability of infection (P_I), for the SARS-CoV-2 virus, has been plotted as a function of ACH for room 1 and room 6 in Figure 7 using the mean value for quantum emission rate ($\mathrm{ER}_q = 970$ quanta/h) and inhalation rate ($\mathrm{IR} = 1\,\mathrm{m}^3/\mathrm{h}$) from Miller et al. [31].

Figures 7(a) and 7(c) plot P_I for room 1 for $t_0 = 5$ and 15 minutes, respectively. The dilution of concentration due to the large volume of the room ($\mathscr{V} = 320\,\mathrm{m}^3$) results in a lower probability of infection at large separation distances even at the worst-case ACH. Figures 7(b) and 7(d) plot P_I for the smaller room 6 for $t_0 = 5$ and 15 minutes, respectively. The smaller volume ($\mathscr{V} = 72.9\,\mathrm{m}^3$) of the room results in a considerably higher value of P_I at separation distances on the order of $0.4L$ (i.e., ≈ 2 m). For such a scenario, as can be seen from Figure 7, moving away from the worst-case ACH can offer significant reduction in the probability of infection.

4. Conclusions

The results of the study indicate the existence of a clear worst-case value of ACH for scenarios where the time of occupation is small and the separation between the occupants with respect to the size of the room is large. This value of worst-case ACH reduces with an increase in time of occupation and a reduction in separation distance. This observation, under conditions where it applies, warrants caution in the application of current standard recommendation of a minimum ventilation rates. In addition, one must also avoid operating close to the worst-case ACH to reduce the risk of infection for airborne diseases.

The guideline for short-term exposure in small- to medium-sized indoor spaces can be summarized as follows. Each person should avoid being in the path of the potentially virus containing puff ejected by the other person while breathing or talking. (This short direct pathway between the sick and the susceptible is not considered in the present study where the focus is on ventilation-driven airborne transmission.) Mixing of air between the two must be prevented with the installation of a divider [40] or promoting separate microventilation units around the sick and the susceptible. If avoiding mixing of air due to ventilation is not possible during the short period when the two individuals are together, it is better to turn off the air-conditioner. This will greatly reduce the probability of infection. Between these short meetings, when the room is unoccupied, the air-conditioner can be operated at a maximum setting to both clean the room of airborne nuclei and set the temperature and humidity to the desired level. Finally, in other scenarios, where the exposure time is long and separation distances are short, occupancy level is high, and the above recommendations will not apply.

Data Availability

The data that support the findings of this study are available from the corresponding author upon reasonable request.

Conflicts of Interest

The authors have no conflicts to disclose.

Authors' Contributions

K.A.K and K.C. conducted the simulations and processed the data. C.Y.C. conducted the experiments. S.B., N.Z., and K.A.K. conceptualized the work. S.B., K.A.K, and N.Z. prepared the manuscript with help from M.Y.H., K.C., C.Y.C., K.S.B, and S.J.

Acknowledgments

We would like to acknowledge the foundational research and insights provided in our previous papers titled "Improved Guidelines of Indoor Airborne Transmission Taking into Account Departure from the Well-Mixed Assumption" [26] and "Fluid Mechanics of Air Recycling and Filtration for Indoor Airborne Transmission" [27], which laid the groundwork for the methodologies discussed in this paper. We gratefully acknowledge support from NSF, USA (EAGER Grant no. 2134083); LG Electronics, Korea (Grant no. C2021017165); DOE/NNSA Minority Serving Institutions Partnership Program under Award No. DE-NA0004003; and the University of Florida Informatics Institute, USA.

References

[1] A. Fontanet and S. Cauchemez, "Covid-19 herd immunity: where are we?," *Nature Reviews Immunology*, vol. 20, no. 10, pp. 583-584, 2020.

[2] N. H. Leung, "Transmissibility and transmission of respiratory viruses," *Nature Reviews Microbiology*, vol. 19, no. 8, pp. 528–545, 2021.

[3] X. Peng, X. Xu, Y. Li, L. Cheng, X. Zhou, and B. Ren, "Transmission routes of 2019-ncov and controls in dental practice," *International Journal of Oral Science*, vol. 12, no. 1, 2020.

[4] S. Moritz, C. Gottschick, J. Horn et al., "The risk of indoor sports and culture events for the transmission of COVID-19," *Nature Communications*, vol. 12, no. 1, p. 5096, 2021.

[5] B. Chen, P. Jia, and J. Han, "Role of indoor aerosols for COVID-19 viral transmission: a review," *Environmental Chemistry Letters*, vol. 19, no. 3, pp. 1953–1970, 2021.

[6] M. Z. Bazant and J. W. Bush, "A guideline to limit indoor airborne transmission of COVID-19," *Proceedings of the National Academy of Sciences*, vol. 118, no. 17, 2021.

[7] K. Nissen, J. Krambrich, D. Akaberi et al., "Long-distance airborne dispersal of SARS-CoV-2 in COVID-19 wards," *Scientific Reports*, vol. 10, no. 1, article 19589, 2020.

[8] R. Zhang, Y. Li, A. L. Zhang, Y. Wang, and M. J. Molina, "Identifying airborne transmission as the dominant route for the spread of COVID-19," *Proceedings of the National Academy of Sciences*, vol. 117, no. 26, pp. 14857–14863, 2020.

[9] S. E. Hwang, J. H. Chang, B. Oh, and J. Heo, "Possible aerosol transmission of COVID-19 associated with an outbreak in an apartment in Seoul, South Korea, 2020," *International Journal of Infectious Diseases*, vol. 104, pp. 73–76, 2021.

[10] L. Morawska, J. W. Tang, W. Bahnfleth et al., "How can airborne transmission of COVID-19 indoors be minimised?," *Environment International*, vol. 142, article 105832, 2020.

[11] M. E. Rosti, S. Olivieri, M. Cavaiola, A. Seminara, and A. Mazzino, "Fluid dynamics of COVID-19 airborne infection suggests urgent data for a scientific design of social distancing," *Scientific Reports*, vol. 10, no. 1, article 22426, 2020.

[12] Y. Liu, Z. Ning, Y. Chen et al., "Aerodynamic analysis of SARS-CoV-2 in two Wuhan hospitals," *Nature*, vol. 582, no. 7813, pp. 557–560, 2020.

[13] P. Y. Chia, K. K. Coleman, Y. K. Tan et al., "Detection of air and surface contamination by SARS-CoV-2 in hospital rooms of infected patients," *Nature Communications*, vol. 11, no. 1, p. 2800, 2020.

[14] M. D. Ramuta, C. M. Newman, S. F. Brakefield et al., "SARS-CoV-2 and other respiratory pathogens are detected in continuous air samples from congregate settings," *Nature Communications*, vol. 13, p. 4717, 2022.

[15] L. Bourouiba, "Turbulent gas clouds and respiratory pathogen emissions: potential implications for reducing transmission of COVID-19," *JAMA*, vol. 323, pp. 1837-1838, 2020.

[16] L. Bourouiba, "A sneeze," *New England Journal of Medicine*, vol. 375, no. 8, article e15, 2016.

[17] F. Yang, A. A. Pahlavan, S. Mendez, M. Abkarian, and H. A. Stone, "Towards improved social distancing guidelines: space and time dependence of virus transmission from speech-driven aerosol transport between two individuals," *Physical Review Fluids*, vol. 5, no. 12, article 122501, 2020.

[18] ASHRAE, *ANSI/ASHRAE standard 62.1-2022, Ventilation for acceptable indoor air quality*, American Society of Heating, Refrigeration and Air-Conditioning Engineers, Inc., Atlanta, GA, 2022.

[19] A. Persily, "Challenges in developing ventilation and indoor air quality standards: the story of ASHRAE Standard 62," *Building and Environment*, vol. 91, pp. 61–69, 2015.

[20] J. C. Luongo, K. P. Fennelly, J. A. Keen, Z. J. Zhai, B. W. Jones, and S. L. Miller, "Role of mechanical ventilation in the airborne transmission of infectious agents in buildings," *Indoor Air*, vol. 26, no. 5, pp. 666–678, 2016.

[21] Y. Li, H. Qian, J. Hang et al., "Probable airborne transmission of SARS-CoV-2 in a poorly ventilated restaurant," *Building and Environment*, vol. 196, article 107788, 2021.

[22] A. Venkatram and J. Weil, "Modeling turbulent transport of aerosols inside rooms using eddy diffusivity," *Indoor Air*, vol. 31, no. 6, pp. 1886–1895, 2021.

[23] Z. Ai, K. Hashimoto, and A. K. Melikov, "Airborne transmission between room occupants during short-term events: measurement and evaluation," *Indoor Air*, vol. 29, 2019.

[24] M. Bertone, A. Mikszewski, L. Stabile et al., "Assessment of SARS-CoV-2 airborne infection transmission risk in public buses," *Geoscience Frontiers*, vol. 13, no. 6, article 101398, 2022.

[25] J. Kurnitski, M. Kiil, A. Mikola et al., "Post-COVID ventilation design: infection risk-based target ventilation rates and point source ventilation effectiveness," *Energy and Buildings*, vol. 296, article 113386, 2023.

[26] J. S. Salinas, K. A. Krishnaprasad, N. Zgheib, and S. Balachandar, "Improved guidelines of indoor airborne transmission taking into account departure from the well-mixed assumption," *Physical Review Fluids*, vol. 7, no. 6, article 064309, 2022.

[27] K. A. Krishnaprasad, J. Salinas, N. Zgheib, and S. Balachandar, "Fluid mechanics of air recycling and filtration for indoor airborne transmission," *Physics of Fluids*, vol. 35, no. 1, 2023.

[28] F. Memarzadeh and W. Xu, "Role of air changes per hour (ach) in possible transmission of airborne infections," *Building Simulation*, vol. 5, no. 1, pp. 15–28, 2012.

[29] W. Wells, *Airborne contagion and air hygiene: an ecological study of droplet infections*, Harvard University Press, 1955.

[30] E. Riley, G. Murphy, and R. Riley, "Airborne spread of measles in a suburban elementary school," *American Journal of Epidemiology*, vol. 107, no. 5, pp. 421–432, 1978.

[31] S. L. Miller, W. W. Nazaroff, J. L. Jimenez et al., "Transmission of SARS-CoV-2 by inhalation of respiratory aerosol in the Skagit Valley Chorale superspreading event," *Indoor Air*, vol. 31, no. 2, pp. 314–323, 2021.

[32] F. Q. Hu, "On absorbing boundary conditions for linearized Euler equations by a perfectly matched layer," *Journal of Computational Physics*, vol. 129, no. 1, pp. 201–219, 1996.

[33] K. Choudhary, K. A. Krishnaprasad, S. Pandey et al., "Effectiveness of rans in predicting indoor airborne viral transmission: a critical evaluation against les," *Computers & Fluids*, vol. 256, article 105845, 2023.

[34] L. Hamner, P. Dubbel, I. Capron et al., "High SARS-CoV-2 attack rate following exposure at a choir practice—Skagit County, Washington, March 2020,," *Morbidity and Mortality Weekly Report*, vol. 69, no. 19, pp. 606–610, 2020.

[35] L. Morawska, G. R. Johnson, Z. Ristovski et al., "Size distribution and sites of origin of droplets expelled from the human respiratory tract during expiratory activities," *Journal of Aerosol Science*, vol. 40, no. 3, pp. 256–269, 2009.

[36] G. Buonanno, L. Stabile, and L. Morawska, "Estimation of airborne viral emission: quanta emission rate of SARS-CoV-2 for infection risk assessment," *Environment International*, vol. 141, article 105794, 2020.

[37] V. F. McNeill, R. Corsi, J. A. Huffman et al., "Room-level ventilation in schools and universities," *Atmospheric Environment: X*, vol. 13, article 100152, 2022.

[38] S. Ferrari, T. Blázquez, R. Cardelli, G. Puglisi, R. Suárez, and L. Mazzarella, "Ventilation strategies to reduce airborne transmission of viruses in classrooms: a systematic review of scientific literature," *Building and Environment*, vol. 222, article 109366, 2022.

[39] D. L. Johnson, R. A. Lynch, E. L. Floyd, J. Wang, and J. N. Bartels, "Indoor air quality in classrooms: environmental measures and effective ventilation rate modeling in urban elementary schools," *Building and Environment*, vol. 136, pp. 185–197, 2018.

[40] W. Hiwar, M. F. King, H. Kharrufa, E. Tidswell, L. A. Fletcher, and C. J. Noakes, "The impact of ventilation rate on reducing the microorganisms load in the air and on surfaces in a room-sized chamber," *Indoor Air*, vol. 32, no. 11, Article ID e13161, 2022.